PHYSICAL REVIEW B **93**, 125207 (2016)

Even-parity excited states of the acceptor boron in silicon revisited

K. J. Morse,[1] R. J. S. Abraham,[1] D. P. Franke,[2] N. V. Abrosimov,[3] and M. L. W. Thewalt[1,*]

[1]*Department of Physics, Simon Fraser University, Burnaby, British Columbia, Canada V5A 1S6*

[2]*Walter Schottky Institut and Physik Department, Technische Universität München, Am Coulombwall 4, D-85748 Garching, Germany*

[3]*Leibniz-Institut für Kristallzüchtung, D-12489 Berlin, Germany*

(Received 5 January 2016; published 10 March 2016)

While the odd-parity electronic excited states of the prototypical acceptor boron in silicon have received detailed experimental and theoretical study, the properties of the even-parity excited states are less well known. Indeed, a recent study has strongly questioned the existing assignment of the first even-parity excited state above the $1\Gamma_8^+$ ground state, and further questioned whether the assigned state is even in the silicon band gap. Here we report the results of electronic Raman scattering spectroscopy, acceptor bound exciton two-hole spectroscopy, and thermally induced infrared absorption spectroscopy, all of which support the original assignment of the lowest-lying even-parity excited state of boron in silicon to the $1\Gamma_7^+$ state associated with the split-off valence band.

DOI: 10.1103/PhysRevB.93.125207

I. INTRODUCTION

Recent proposals to use the electronic states of acceptor impurities in silicon as active laser media [1] and as qubits for a semiconductor-based quantum information technology [2] require detailed knowledge of the ground- and excited-state properties of these systems. Transitions from the even-parity $1\Gamma_8^+$ ground state to odd-parity excited states of shallow acceptors are dipole-allowed, and readily observed by infrared (IR) absorption spectroscopy. As a result, these states have been the subject of many highly detailed studies, both theoretical and experimental, since they were first discovered in silicon [3], as reviewed recently by Pajot [4]. Transitions to the even-parity excited states are dipole-forbidden, and as a result much less is known about them. A Raman-active transition at ∼22.7 meV (∼183 cm^{-1}) in boron-doped silicon has long been thought to arise from a transition to the $1\Gamma_7^+$ state associated with the split-off valence band, making it the lowest energy even-parity excited state [5–8]. However, this assignment has now been strongly questioned, and it has been further asserted that the $1\Gamma_7^+$ state may not even lie in the silicon band gap [1]. The importance of this controversy goes well beyond the potential applications of boron excited states for terahertz lasers or quantum information, since boron in silicon, the most thoroughly studied acceptor in the most thoroughly studied semiconductor, is the prototypical acceptor. Here we report the results of Raman scattering spectroscopy, bound exciton two-hole photoluminescence spectroscopy, and thermally induced infrared absorption spectroscopy, confirming the original assignment of $1\Gamma_7^+$ as the deepest even-parity excited state of boron in silicon.

Wright and Mooradian [5] were the first to report a Raman feature at 23.4 meV (188.7 cm^{-1}) in boron-doped silicon, ascribing it to an even-parity electronic excited state, and later proposing [6] that the state could have a 1*s*-like envelope function together with states from the split-off $p_{1/2}$ valence band edge. This possibility was supported by Raman scattering studies under uniaxial strain and magnetic fields, which were consistent with transitions from the fourfold-degenerate $1\Gamma_8^+$ ground state to a doubly degenerate excited state having either Γ_6 or Γ_7 symmetry, and which also gave a slightly different value of 22.7 meV (183.1 cm^{-1}) for the energy of the unperturbed Raman feature [9]. That the Raman feature was indeed due to the $1\Gamma_7^+$ state associated with the split-off band valence band was supported by theoretical calculations showing that for boron this state would be located in the silicon band gap, at very near the observed energy above the $1\Gamma_8^+$ ground state [7,8].

This has recently been called into question by Pavlov *et al.* [1] in a study of stimulated emission from boron in silicon when pumping the $1\Gamma_8^+$ to odd-parity excited state transitions resonantly using a free electron laser. Emission was only observed from odd-parity excited states to the $2\Gamma_8^+$ even-parity state, even though this state lies above the location claimed for $1\Gamma_7^+$, and on the basis of this observation and other arguments Pavlov *et al.* [1] concluded that $2\Gamma_8^+$ was the deepest even-parity excited state of boron, and that the $1\Gamma_7^+$ state did not lie ∼183 cm^{-1} above the $1\Gamma_8^+$ ground state, and in fact might not even lie in the silicon band gap. The other arguments used to reach this conclusion were that no emission from odd-parity states to $1\Gamma_7^+$ was observed in the electroluminescence of boron in silicon [10], and that the $1\Gamma_7^+$ state was not observed in the boron acceptor bound exciton (A^0X) two-hole photoluminescence (PL) transitions, which have been used to observe the $n\Gamma_8^+$ ($n > 1$) even-parity excited states of boron in silicon [11–13]. Pavlov *et al.* [1] also noted that the Raman scattering experiments of Wright and Mooradian [5,6] and of Cherlow *et al.* [9] both used 1064 nm Nd:YAG laser excitation as a source, and that this could have led to spurious results due to the near resonance of the laser energy with the silicon band gap energy. Pavlov *et al.* [1] pointed out that a weak infrared absorption feature observed at 22.77 meV (183.7 cm^{-1}) in heavily boron-doped silicon by Chandrasekhar *et al.* [14] and attributed to the $1\Gamma_7^+$ level could instead be due to the first dipole-allowed transition of the boron-*X* acceptor reported by Scott and Jones [15]. Finally, they stated that no thermally induced infrared absorption could be observed at elevated temperatures in boron-doped silicon arising from transitions from a thermally populated $1\Gamma_7^+$ level

*Corresponding author: thewalt@sfu.ca

to higher-lying odd-parity excited states, in analogy to the thermally induced absorption used previously to observe the $1s(T_2)$ and $1s(E)$ even-parity valley-orbit excited states in donor-doped silicon [16].

Given the previously well-established consensus on the existence of the $1\Gamma_7^+$ level $\sim$183 cm^{-1} above the $1\Gamma_8^+$ ground state, we have further investigated the results and arguments of Pavlov *et al.* [1] While we are not equipped to replicate their stimulated emission experiment, neither do we question this central experimental result. A possible explanation for the failure to observe stimulated emission with $1\Gamma_7^+$ as a final state could be a low oscillator strength for these transitions, which would also explain the absence of any final state other than the $1\Gamma_8^+$ ground state in the earlier electroluminescence spectra [10]. We will later show that these transitions involving $1\Gamma_7^+$ do indeed have lower oscillator strength than transitions between $n\Gamma_8^+$ even-parity states and the odd-parity excited states. The suggestion of possible spurious Raman scattering results when using a 1064-nm laser due to resonance effects is already addressed by the fact that Serrano *et al.* [17] observed the same electronic Raman scattering feature at 22.8 meV (183.9 cm^{-1}) in boron-doped silicon when using 799.3-nm laser excitation, well above the silicon band gap and far from any resonance. Nevertheless, we thought it worthwhile to replicate the Raman results using a 1081-nm laser, well below the silicon band gap, and in fact below the energies of any of the shallow bound exciton states in silicon. The results are very similar to the 1064-nm results, except for the absence of the weak boron bound exciton PL features which are present when using 1064 nm, since that laser energy is slightly above the no-phonon free exciton absorption edge of silicon. In addition to the dominant 183.5(2) cm^{-1} $1\Gamma_7^+$ feature, we also observe electronic Raman scattering involving several higher-lying even-parity electronic excited states.

The so-called acceptor bound exciton two-hole transitions provide another means of observing even-parity acceptor excited states, and we reinvestigate these using both the previously studied [13] transverse optical (TO) wave-vector-conserving phonon replica PL, as well as the no-phonon PL, which is very weak for boron. In two-hole PL spectroscopy, the acceptor excited state energy is given by the energy difference between the principal A^0X transition, which leaves the acceptor in its ground state, and the weaker two-hole transitions, which leave the acceptor in an electronic excited state. These transitions reflect the fact that while the wave functions of the two holes in the A^0X ground state are still $1s$-like, they must have a larger spatial extent than that of the neutral acceptor (A^0) ground state, and hence the two-hole transitions show the degree of overlap between the ground-state hole wave function of A^0X and the excited state wave functions of A^0. We again find no evidence for $1\Gamma_7^+$ in the A^0X two-hole PL spectra, but this is not an argument against the existence of the $1\Gamma_7^+$ state, since Raman scattering and two-hole replica PL transitions can have quite different selection rules. This is demonstrated by other interesting differences in some of the higher-lying even-parity excited states revealed in our Raman scattering and two-hole A^0X PL results.

We are in agreement with Pavlov *et al.* [1] that the weak absorption feature reported by Chandrasekhar *et al.* [14] at 22.77 meV in a heavily boron-doped sample is likely not due to $1\Gamma_7^+$, but rather to the accidentally degenerate line 1 of the boron-X center [15]. In two different samples of heavily boron-doped silicon, we observe this feature at the same strength relative to the normal boron absorption lines, and we also observe lines 2, 3, and 4 of the previously reported boron-X [15] series at the appropriate relative intensities, strongly supporting the identification of the 22.77-meV absorption feature as being due to boron-X.

The strongest argument against $1\Gamma_7^+$ being the deepest even-parity excited state of boron in silicon was the inability to observe any thermally induced absorption from this state to higher-lying odd-parity states at elevated temperatures [1]. This is, however, a more difficult measurement than the previously demonstrated thermally induced absorption due to the $1s(E)$ and $1s(T_2)$ states of donors [16], since for boron the expected $1\Gamma_7^+$ energy is fully one-half of the boron ionization energy. The large effective valence band density of states at temperatures of tens of Kelvins, compared to the usable boron concentration, results in significant boron ionization at the temperatures needed to obtain even small populations in the $1\Gamma_7^+$ level, which in turn leads to strong free carrier absorption in the spectral region of interest. We were nevertheless able to observe thermally induced absorption features by using long path lengths and heavily boron-doped samples. These features first become visible at 25 K, and grow in strength to 50 K, where the sample becomes effectively opaque due to free carrier absorption. Thermally induced absorption was observed not only from $1\Gamma_7^+$ but also from the higher-lying $1\Gamma_8^-$ and $2\Gamma_8^+$ initial states. Taken together these results strongly support the original assignment of $1\Gamma_7^+$ as the deepest even-parity excited state of the boron acceptor in silicon, lying 183.5(2)cm^{-1} above the $1\Gamma_8^+$ ground state.

II. SAMPLES AND METHODS

The samples used in this work for the liquid He temperature infrared absorption spectroscopy, the temperature-induced infrared absorption spectroscopy, and the electronic Raman scattering spectroscopy were cut from two floating-zone grown silicon crystals doped with 5×10^{16}cm^{-3} of boron. The first crystal, hereinafter referred to as A, had an unknown carbon content, and to investigate the possible influence of carbon on the boron-X concentration a new crystal B was grown using high-purity starting material and five floating-zone passes to further reduce any carbon contamination. While the data shown here are from B material, it should be emphasized that no significant differences were observed between A and B samples in any aspect of the low temperature or elevated temperature infrared absorption spectra, nor in the Raman scattering spectra. In order to distinguish between electronic Raman scattering due to boron, and phonon-related Raman scattering, a Raman scattering sample was also fabricated from ultra-high-purity undoped floating-zone grown silicon.

Temperature-induced infrared absorption spectra were obtained using a 30-mm path length sample of crystal B and a 20-mm path length sample of crystal A. The temperature of these samples was not measured directly, but they had large surface areas ($>$ 10 cm^2) in close contact with a temperature controlled Cu block, and the sample temperature was assumed

to be equal to the block temperature given the high thermal conductivity of the He gas ambient at atmospheric pressure, and the low heat load on the samples. For the liquid He temperature infrared absorption spectra of the main boron and boron-X lines, thinner samples of both crystals A and B were prepared, with thicknesses of 3.0, 1.0, and 0.3 mm. In order to see the main boron lines without saturation, a sample of crystal B was further thinned to ∼34 μm by etching in HF/HNO_3. The A and B material was not suitable for studying the boron A^0X PL transitions, since due to the high boron concentration the PL spectrum was dominated by luminescence from excitons localized on boron clusters, producing a broad signal lying at lower energy than the weaker isolated boron A^0X line, which could still be observed in these samples. Instead, boron A^0X PL spectra showing the two-hole transitions were obtained from a more lightly doped floating-zone grown sample of silicon containing $3 \times 10^{15}\text{cm}^{-3}$ boron.

All of the spectroscopy was carried out using a Bruker IFS 125HR Fourier transform infrared (FTIR) spectrometer. The infrared absorption spectroscopy was performed with a Mylar beamsplitter having a multilayer coating optimized for the 50–600 cm^{-1} spectral region, either a Globar or Hg arc lamp source, and a 4.2-K silicon bolometer detector using either a 100-cm^{-1} or 800-cm^{-1} low-pass cold filter, depending upon the spectral region of interest.

The PL and Raman scattering spectroscopy were performed with a CaF_2 beamsplitter and a high sensitivity liquid nitrogen cooled germanium detector. For the PL spectroscopy, the sample was excited with 300 mW of light at 1030 nm from a laser diode source, providing quasibulk excitation and a large PL signal. A long-pass interference filter was used to block the excitation light when collecting the relatively strong TO phonon replica PL, and an additional band-pass interference filter was used in order to obtain an improved signal-to-noise ratio (SNR) when collecting the weaker no-phonon PL. Raman spectra were collected using both 1064-nm and 1081-nm single-frequency lasers with sub-MHz linewidths. In both cases the lasers first passed through narrow band-pass laser cleanup filters, and the laser radiation was separated from the Raman scattering signal before entering the FTIR using sharp cutoff laser rejection long-pass interference filters. The 1064-nm Raman scattering was performed with 200 mW of light from a single-frequency diode-pumped Nd:YAG laser, while the 1081-nm Raman scattering used 700 mW of light from a single-frequency distributed feedback Yb-doped fiber laser followed by a Yb-doped fiber amplifier. All three lasers had beam spot sizes at the sample of ∼3 mm.

For all measurements the samples were cooled in Varitemp dewars, either in flowing He gas for $T > 5$ K, or immersed in superfluid He at $T \approx 1.5$ K. For $T > 5$ K the samples were mounted on Cu temperature-controlled stages, with T monitored by a calibrated Si diode sensor and controlled by a heater on the temperature-controlled block. Despite the high power of the 1081-nm laser, heating of the sample was not an issue as the sample is quite transparent at that wavelength. The dewar used for the PL and Raman scattering spectroscopy had fused silica windows, while the dewar used for the infrared absorption spectroscopy had polypropylene film windows.

Except for the liquid He temperature absorption spectroscopy of the main boron and boron-X lines, which was done at a spectral resolution of 0.25 cm^{-1}, all of the spectra reported here were weak and required a tradeoff between spectral resolution and SNR. The Raman and PL spectra were collected at a spectral resolution of 0.5 cm^{-1}, and the thermally induced infrared absorption spectroscopy was collected at a spectral resolution of 1 cm^{-1}.

III. RESULTS

A. Low temperature infrared absorption

Infrared absorption spectra from the acceptor ground state $1\Gamma_8^+$ to odd-parity excited states for the low-carbon crystal B doped with $5 \times 10^{16}\,\text{cm}^{-3}$ boron are shown in Fig. 1. Due to the relatively heavy doping, the sample had to be thinned to ∼34 μm by etching so as not to saturate the stronger absorption lines. Due to the nonuniform sample thickness, the absorption coefficient values are only approximate, but they agree with earlier results [18] when corrected for the higher doping. The boron features are labeled 1,2,3 using the scheme given by Ramdas and Rodriguez [18], although our line 4 is actually lines 4, 4B, and 4A, which are unresolved here due to concentration broadening. This line numbering scheme has evolved over time and suffers from inconsistencies between different authors as discussed by Pajot [4], so the transition energies are given in Table I both in terms of these line numbers and in terms of the symmetry label of the excited state involved in the transition.

Also shown in Fig. 1 is the absorption spectrum of a 1-mm thick sample of the same material, revealing weaker features labeled 1′, 2′, 3′, 4′ whose energies and relative intensities are essentially identical to the absorption features of the boron-X center as reported by Scott and Jones [15]. The absorption spectrum of sample A, which likely contained significantly more carbon contamination, showed the identical 1′ to 4′

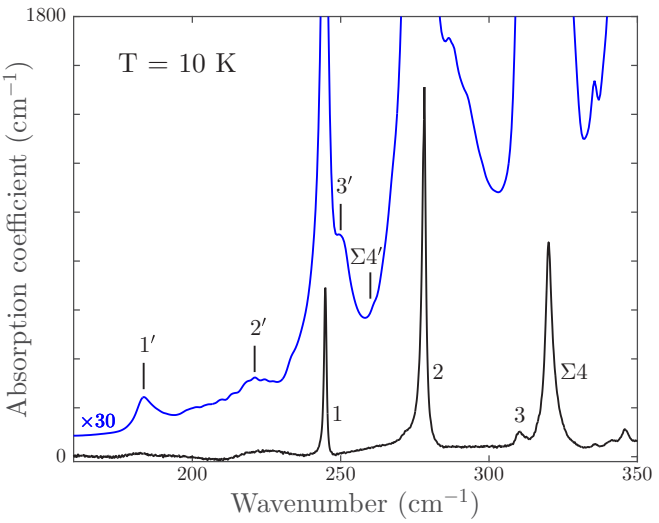

FIG. 1. Infrared absorption spectra of silicon doped with $5 \times 10^{16}\,\text{cm}^{-3}$ boron. The bottom spectrum, showing the main boron lines 1 to Σ4 (comprising the unresolved lines 4, 4B, and 4A), is from a sample thinned to approximately 34 μm, while the top spectrum, showing the 1 to Σ4 lines of the boron-X center (labeled with primes), is from a 1-mm thick sample.

TABLE I. Excited state energies for boron measured from the $1\Gamma_8^+$ ground state. The IR energies are taken from a high resolution study using lightly doped samples [19], and both the line numbers (in parentheses) and excited state symmetry labels are given for these. Also tabulated are the excited state energies determined here using electronic Raman scattering and bound exciton two-hole PL spectroscopy.

	Excitation Energy (cm^{-1})		
Excited state	IR	Raman	NP PL
$1\Gamma_7^+$		183.5(2)	
$1\Gamma_8^-$ (1)	244.946	244.8(2)	245.0(5)
$2\Gamma_8^+$		261.2(3)	261.4(2)
$2\Gamma_8^-$ (2)	278.295	278.1(3)	278.4(2)
$3\Gamma_8^-$ (3)	309.531		
$3\Gamma_8^+$a		315.8(3)	
$3\Gamma_8^+$b			317.3(2)
$1\Gamma_6^-$ (4)	319.374		
$1\Gamma_7^-$ (4B)	320.032		
$4\Gamma_8^-$ (4A)	321.910		
$1\Gamma_6^+$		327.1(4)	
$4\Gamma_8^+$		337.8(5)	338.1(2)
$5\Gamma_8^+$		348.4(8)	348.3(4)

features, and at the same relative intensity to the normal boron features. This calls into question the proposal [20] that the acceptor-X centers are due to acceptor-carbon pairs, which has already been questioned for the case of gallium-X [21]. In any case, in both our samples the $1'$ line at $\sim$184 cm^{-1} can be completely accounted for by boron-X absorption, supporting the suggestion by Pavlov *et al.* [1] that the earlier attribution [14] of a feature at the same energy to a boron $1\Gamma_8^+$ to $1\Gamma_7^+$ transition was mistaken.

B. Raman scattering

In order to test the proposal of Pavlov *et al.* [1] that the use of 1064-nm excitation in the earlier [5,6] Raman studies of the $\sim$183 cm^{-1} feature could have led to erroneous results due to resonance effects, we have collected Fourier-transform (FT) Raman spectra of silicon doped with $5 \times 10^{16} cm^{-3}$ boron using both 1064-nm and 1081-nm excitation. When using 1064-nm excitation with this heavily doped sample, the sample temperature had to be increased to $\sim$40 K in order to suppress strong PL from excitons bound to boron clusters. Even at 40 K, there was interference from boron A^0X PL when using 1064-nm excitation, since the transverse acoustic (TA) phonon replica of the boron A^0X transition lies in the region of boron electronic Raman scattering. The problem with PL was expected, since 1064 nm is above the free exciton no-phonon absorption edge of Si at liquid He temperature, while 1081 nm is below the free exciton edge and the ground states of all shallow bound excitons. Since the 1081-nm spectrum was free of any interference from PL, and had better SNR due to the higher laser power, we show only this spectrum in Fig. 2. Other than the PL interference, the 1064-nm and 1081-nm Raman spectra were identical, showing all the same features, and at the same relative intensities.

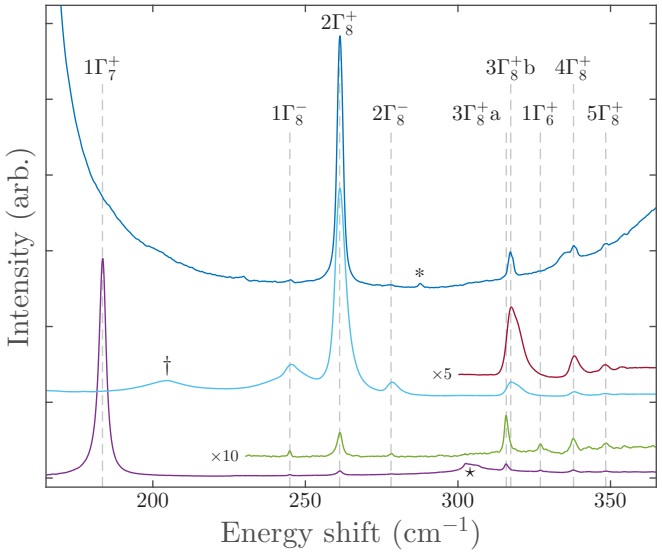

FIG. 2. The bottom spectra shows Raman scattering from a silicon sample doped with 5×10^{16} cm^{-3} boron, using 1081-nm laser excitation. The weaker features are shown expanded by a factor of 10, and with the 2-TA phonon Raman feature, labeled with a ⋆, removed. The middle spectrum shows the TO-phonon replica acceptor bound exciton two-hole PL of a silicon sample doped with $3 \times 10^{15} cm^{-3}$, while the top spectrum shows the two-hole PL of the same sample in the no-phonon region. The weak feature labeled with a ∗ is the no-phonon two-electron 2s replica due to a small phosphorus contamination in the sample.

As seen in Fig. 2 (bottom trace), the $1\Gamma_7^+$ Raman scattering at 183.5(2)cm^{-1} dominates the electronic Raman scattering spectrum, although it is a factor of $\sim$60 weaker than the zone-center optical phonon scattering at 524 cm^{-1}, which is not shown. A feature at $\sim$305 cm^{-1} and labeled with a ⋆ in Fig. 2 (bottom trace) was also seen in earlier Raman spectra [5]. This results from multiphonon scattering, reflecting a peak in the two-TA phonon density of states [22]. This feature has been removed from the second trace from the bottom in Fig. 2 by subtracting the Raman spectrum of an undoped silicon sample. In addition to the $1\Gamma_7^+$ line, other weaker electronic Raman scattering to higher-lying excited states is observed, including very weak scattering due to $1\Gamma_8^-$ and $2\Gamma_8^-$ odd-parity excited states, and scattering from higher even-parity states which has not been reported previously. All of the electronic Raman transition energies are summarized in Table I.

C. Boron bound exciton two-hole PL transitions

The even-parity boron excited states $2\Gamma_8^+$ through $5\Gamma_8^+$ have been observed previously using boron A^0X two-hole PL spectroscopy in the relatively strong TO phonon replica region [13], and identified by comparison with theoretical binding energies [11,12]. The observation by Pavlov *et al.* [1] that the $1\Gamma_7^+$ state was not reported in these spectra, even though it dominates the electronic Raman scattering spectrum, caused us to reexamine these transitions both in the previously studied TO phonon replica region, as well as in the much weaker (for boron) no-phonon PL region. The TO phonon-replica PL suffers from unavoidable phonon-related

broadening [23], which is absent in the no-phonon PL process, providing higher spectral resolution.

The spectrum in the TO phonon-replica region is shown as the central trace in Fig. 2, where the energy shift is measured from the center of the principal bound exciton transition. It is essentially the same as the earlier result [13], but with improved spectral resolution and SNR. The feature marked with a † was identified as a two-phonon (TO wave-vector-conserving phonon plus $\delta 1$ intervalley scattering phonon) replica of the principal bound exciton transition [13]. As before [13], relatively strong odd-parity replicas are seen involving the $1\Gamma_8^-$ and $2\Gamma_8^-$ states, and a shoulder on the high-energy side of the $3\Gamma_8^+$ line likely results from unresolved transitions to $1\Gamma_6^-$, $1\Gamma_7^-$ and $4\Gamma_8^-$ (line $\Sigma 4$). There is no sign of a transition to a $1\Gamma_7^+$ final state.

This is also true of the no-phonon A^0X two-hole transition spectrum shown as the top trace of Fig. 2. The transitions to odd-parity excited states are almost undetectable in the no-phonon spectrum, indicating that their presence in the TO-replica spectrum results from relaxation of selection rules due to phonon participation. While the $2\Gamma_8^+$ line is broadened by final state lifetime broadening, the higher Γ_8^+ states are sharper and reveal unresolved structure which can also be observed in the no-phonon boron A^0X principal transition at this spectral resolution [24]. This is very similar to the situation seen in IR absorption to the odd-parity states, where the deeper states have much larger lifetime broadenings than do the higher excited states [19].

In comparing the Raman and two-hole spectra in Fig. 2 it is noteworthy that the $2\Gamma_8^+$ energy shifts agree very well, while the $3\Gamma_8^+$ shifts are distinctly different, and have been labeled $3\Gamma_8^+$a for the Raman feature and $3\Gamma_8^+$b for the two-hole feature. A possible explanation for this is discussed in the following section. There are signs of a similar but smaller difference in the $4\Gamma_8^+$ lines, but since this was less than the spectral resolution, we do not distinguish between the features in the Raman and two-hole spectra. All of the excited state energies observed in the Raman scattering and A^0X two-hole spectra are summarized in Table I.

D. Infrared absorption from thermally populated initial states

To find further evidence of the $1\Gamma_7^+$ state we investigated the infrared absorption spectrum of thick samples of silicon doped with 5×10^{16}cm^{-3} of boron, looking for the expected transitions from the thermally populated $1\Gamma_7^+$ state to the shallower odd-parity states. At temperatures below 20 K there was essentially no absorption below the ~184-cm^{-1} line which we have previously ascribed to line 1 of the boron-X center, so the 20-K spectrum was used as a reference for calculating the temperature-induced absorbance at higher temperatures. The presence of the boron-X absorption (and the even stronger higher energy boron absorption) rendered these thick and relatively heavily doped samples effectively opaque from below the ~184-cm^{-1} line to above 800 cm^{-1}, so the temperature-induced absorption could only be studied below ~150 cm^{-1}.

New temperature-induced absorption features became observable above 25 K, and the results from 30 to 50 K are shown in Fig. 3. In addition to the lines observed in Fig. 3, above 20 K a growing free carrier absorption appeared, which increased in strength with decreasing photon energy. This free carrier absorption rendered the sample effectively opaque in the spectral region of interest above 50 K.

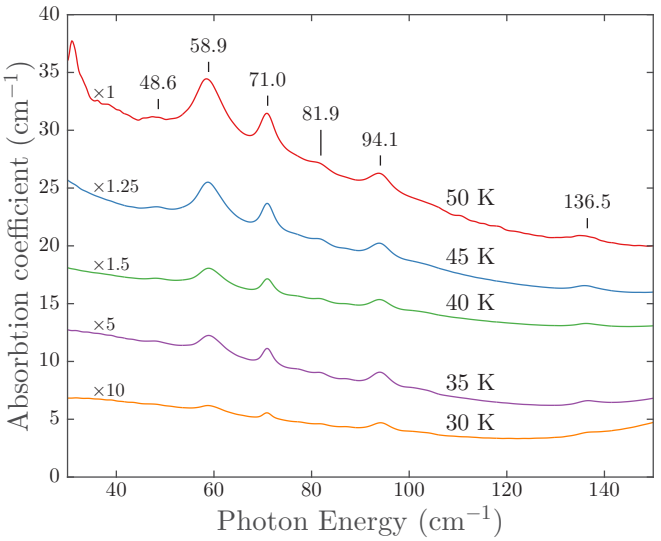

FIG. 3. Thermally induced infrared absorption spectra in a 30-mm thick sample containing 5×10^{16}cm^{-3} boron.

Six temperature-induced absorption transitions were clearly observable at all temperatures between 25 and 50 K, and are labeled in Fig. 3 by their transition energies. The proposed origin of these six temperature-induced transitions is shown in Fig. 4, and the observed and predicted energies are summarized in Table II. It is clear from Fig. 3 that the relative intensities of some of the lines changed noticeably with temperature, so the areas of the stronger lines were determined as a function of temperature and shown as an Arrhenius plot

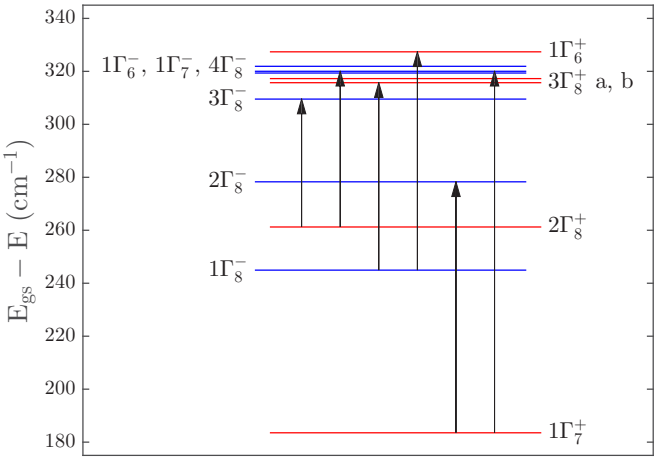

FIG. 4. Level diagram illustrating the assigned origins of the thermally induced absorption lines, from lowest energy (48.6 cm^{-1}) on the left to highest energy (136.5 cm^{-1}) on the right. The $1\Gamma_8^+$ acceptor ground state is at zero energy on this scale, while the ionization edge (the degenerate light and heavy hole valence band edges) is at 368 cm^{-1} and the split-off valence band edge in silicon lies ~355 cm^{-1} above that.

TABLE II. Summary of line positions observed for transitions from thermally populated states. Predicted energies are the energy differences of the assigned levels according to Table I. All energies are in cm^{-1}.

Energy	Predicted Energy	Assignment	Activation Energy	Predicted Activation Energy
48.6(4)	48.20(18)	$2\Gamma_8^+ \rightarrow 3\Gamma_8^-$		
58.9(4)	58.04(18), 58.70(18), 60.58(18)	$2\Gamma_8^+ \rightarrow 1\Gamma_6^-, 1\Gamma_7^-, 4\Gamma_8^-$	255(14)	261.33(18)
71.0(2)	70.9(3), 72.4(2)	$1\Gamma_8^- \rightarrow 3\Gamma_8^+$a, $3\Gamma_8^+$b	238(13)	244.946
81.9(2)	82.2(4)	$1\Gamma_8^- \rightarrow 1\Gamma_6^+$		
94.1(2)	94.8(2)	$1\Gamma_7^+ \rightarrow 2\Gamma_8^-$	169(10)	183.5(2)
136.5(3)	135.9(2), 136.5(2), 138.4(2)	$1\Gamma_7^+ \rightarrow 1\Gamma_6^-, 1\Gamma_7^-, 4\Gamma_8^-$	200(17)	183.5(2)

in Fig. 5. The activation energies determined from linear fits to this data are also given in Table II, and compared to the expected activation energies.

The agreement between both the predicted and observed transition energies and activation energies is quite good. There is considerable uncertainty in the activation energy of the 136.5-cm^{-1} transition as it was relatively weak, and located at an energy where the background curvature was changing with temperature, making the separation of line and background difficult. Not all possible transitions are observed, and in particular one might have expected to observe the $1\Gamma_7^+$ to $1\Gamma_8^-$ transition at ~61.5 cm^{-1}, but it may simply have a much smaller oscillator strength than the nearby 58.9-cm^{-1} transition, even though the latter has a larger activation energy. The small disagreement in the predicted and observed energies for the 94.1-cm^{-1} line could arise from a small, unresolved component of $1\Gamma_8^-$ to $4\Gamma_8^+$, which has a predicted energy of 92.9(5)cm^{-1}.

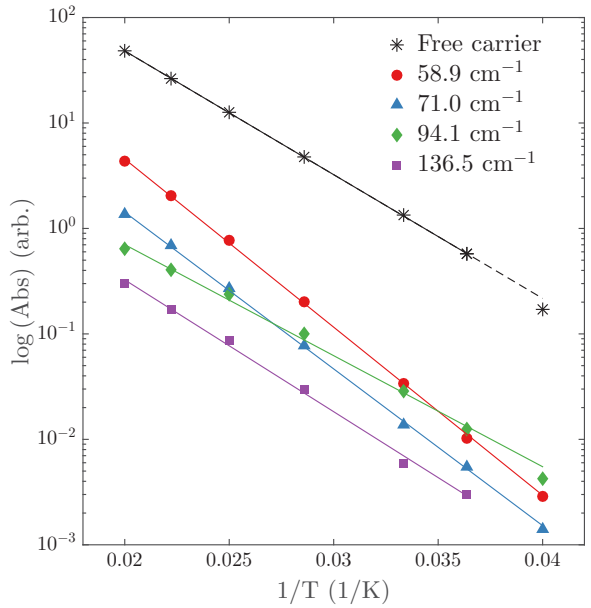

FIG. 5. Arrhenius plot showing the temperature dependence of the stronger thermally induced absorption lines, and the free-carrier absorption. For the absorption lines, areas obtained from fits to the spectra were used, while for the free-carrier absorption the data points are the absorbance at ~115 cm^{-1} multiplied by $T^{-3/4}$. The straight lines represent fits to the data, with resulting activation energies given in Table II.

The absorption versus temperature data can also be used to verify that the origin of the broad, featureless background is due to free holes thermally ionized from the boron. In the extrinsic limit the free hole concentration p is given by

$$p \propto T^{3/4} \exp(-E_{\text{ion}}/2k_{\text{B}}T), \tag{1}$$

where k_{B} is the Boltzmann constant and E_{ion} is the ionization energy [25]. Assuming that the free carrier absorption is linearly proportional to the free hole concentration, we plot the log of the absorption coefficient at 115 cm^{-1} multiplied by $T^{-3/4}$ in Fig. 5. The linear fit to the data points above 25 K gives a thermal ionization energy of 47(2) meV, in excellent agreement with the known ionization energy of boron. The noticeable deviation of the 25-K data point from the linear fit could indicate that the sample is beginning to switch to intrinsic behavior at this temperature [25].

Another noteworthy aspect of the thermally induced absorption lines shown in Fig. 3 is the fact that the 71.0-cm^{-1} line is considerably narrower than the other strong features. This can be understood in terms of the linewidths of the initial and final states of all of these transitions, as summarized in Table III. Note that the full width at half maxima (FWHM) given in the table are the actual observed results, uncorrected for instrumental resolution. The predicted FWHM given in Table III is simply the square root of the sum of the squares

TABLE III. Observed widths for the initial states and final states assigned to the thermally induced transitions, and the widths of the thermally induced transitions themselves. The widths have not been corrected for instrumental resolution. The predicted widths are simply the square root of the sum of the squares of the initial and final state widths.

State/Transition	Observed FWHM (cm^{-1})	Predicted FWHM (cm^{-1})
$1\Gamma_7^+$	2.8	
$1\Gamma_8^-$ (1)	1.0	
$2\Gamma_8^+$	2.0	
$2\Gamma_8^-$ (2)	1.5	
$3\Gamma_8^+$a	1.5	
$1\Gamma_6^-, 1\Gamma_7^-, 4\Gamma_8^-$ ($\Sigma 4$)	2.9	
$2\Gamma_8^+ \rightarrow \Sigma 4$ (58.9)	5.2	3.5
$1\Gamma_8^- \rightarrow 3\Gamma_8^+$a (71.0)	2.2	1.8
$1\Gamma_7^+ \rightarrow 2\Gamma_8^-$ (94.1)	3.9	3.2
$1\Gamma_7^+ \rightarrow \Sigma 4$ (136.5)	4.0	4.0

of the initial and final state FWHM. The predicted widths give a clear indication of why the observed width of the 71.0-cm^{-1} transition should be less than that of the others, although the widths of transitions involving the unresolved $\Sigma 4$ multiplet could vary due to different weightings of its three components.

IV. DISCUSSION

The assignment of the 58.9-cm^{-1} thermally induced absorption feature in Table II and Fig. 4 as $2\Gamma_8^+$ to $\Sigma 4$ means it is the same set of transitions that gave rise to stimulated emission in the work of Pavlov *et al.* [1]. Our temperature-induced absorption results, and in particular the data shown in Fig. 3, allow us to test our earlier hypothesis that transitions from odd parity states to $1\Gamma_7^+$ were not observed in the work of Pavlov *et al.* [1] or in electroluminescence [10] simply because these transitions have low oscillator strength. By extrapolating the linear fits to the absorption feature areas shown in Fig. 5 to $1/T = 0$ we can eliminate thermal population effects and compare the relative oscillator strengths of the transitions. In that limit the areas of the 58.9- and 94.1-cm^{-1} lines are 5.4×10^4 cm^{-2} and 6.9×10^2 cm^{-2}, respectively. Transitions between the $\Sigma 4$ odd parity states and $2\Gamma_8^+$ are seen to be ~75 times stronger than transitions to $1\Gamma_7^+$, supporting our hypothesis. While the oscillator strengths for transitions between the $1\Gamma_8^+$ ground state and many of the odd-parity excited states have been calculated [8,26] there are at present no theoretical estimates of oscillator strengths for transitions between excited states.

Similarly, we are not aware of any theoretical estimates of the relative strengths of acceptor bound exciton two-hole transitions to different final states. In the simplest picture this would be proportional to the overlap of the wave function of the 1*s*-like hole state of the bound exciton ground state and the wave functions of the various acceptor final states, which would suggest only *s*-like even-parity final states. This, however, does not explain the relatively strong odd-parity final states seen in the phonon-assisted bound exciton two-hole transitions. The complete absence of the $1\Gamma_7^+$ state in both the observed no-phonon and phonon-assisted two-hole transitions remains at this point unexplained.

Finally, we consider the differences between the even-parity excited states revealed by Raman scattering and those observed in the A^0X two-hole transitions (other than the dominance of $1\Gamma_7^+$ in Raman scattering, and its absence in the two-hole spectra). The clearest example of this is the apparently distinct $3\Gamma_8^+$ states observed in the two spectroscopies, which we have labeled $3\Gamma_8^+$a in the Raman spectrum and $3\Gamma_8^+$b in the two-hole spectrum. A clue as to the origin of this splitting comes from the $2\Gamma_8^+$ state, which has the same energy in the Raman and two-hole spectra. There exists only a single, *s*-like, $2\Gamma_8^+$ state, but $3\Gamma_8^+$ (and higher) can have either *s*-like or *d*-like envelope functions [8,11]. Theory cannot be used to order the $3\Gamma_8^+$ states, since the two available calculations disagree on this ordering [8,11], but based on our understanding of the two-hole transitions we can propose that $3\Gamma_8^+$b is the *s*-like state.

In order to compare our observed even-parity excited state energies with the theoretically calculated [8,11] binding energies in Table IV, we convert our observed transition energies into binding energies using the 368.0-cm^{-1} ground-state binding energy for boron, as discussed by Pajot [4]. It is on the basis of the agreement with the calculated binding energy for the $1\Gamma_6^+$ state given in [11] that we assigned the Raman feature at 327.1 cm^{-1} to this state in Table I, and in our assignment for the thermally induced absorption feature at 81.9 cm^{-1}.

TABLE IV. Comparison of theoretical and measured binding energies of even-parity excited states. As explained in the text, we associated the $3\Gamma_8^+$a state, observed in Raman scattering, with the *d*-like state and the $3\Gamma_8^+$b state, observed in NP PL, with the *s*-like state. The *s*-*d* splitting could not be resolved in $4\Gamma_8^+$. All energies are in cm^{-1}.

	Theory		
Excited State	[8]	[7,11]	Experiment
$1\Gamma_7^+$	177.0	176.0	184.5
$2\Gamma_8^+$	107.6	108.4	106.8
$3\Gamma_8^+$ *d*	51.2	54.3	52.2
$3\Gamma_8^+$ *s*	54.4	51.5	50.7
$1\Gamma_6^+$	43.1		40.9
$4\Gamma_8^+$ *d*	30.3	31.9	30.2
$4\Gamma_8^+$ *s*	32.0	31.1	–
$4\Gamma_8^+$ *d*	29.8	30.4	–
$5\Gamma_8^+$		21.8	19.6

V. CONCLUSIONS

We have verified the existence of a dominant feature at 183.5(2)cm^{-1} in the electronic Raman scattering spectrum of boron in silicon using an excitation laser wavelength of 1081 nm, placing the photon energy below the silicon band gap, and below the energy of the ground states of shallow bound excitons in silicon, thus eliminating any possibility of resonance effects. The same state was observed as an even-parity initial state in the thermally induced absorption spectrum in heavily-boron-doped silicon, along with transitions from $2\Gamma_8^+$ and $1\Gamma_8^-$ initial states. Taken together, our results strongly support the original interpretation of the ~183-cm^{-1} Raman feature as being due to the $1\Gamma_7^+$ state associated with the split-off valence band, and confirm that this state is the deepest even-parity excited state of boron in silicon. While they do exist, transitions between this state and higher-lying odd-parity states are found to have very low oscillator strength, explaining the absence of these transitions in previous emission or stimulated emission spectra.

We have also observed new features in the Raman spectra and the acceptor bound exciton two-hole transitions which are related to even-parity acceptor excited states, and which may distinguish between *s*-like and *d*-like states associated with $3\Gamma_8^+$. While the $1\Gamma_7^+$ state is now well established for boron, the situation for the other shallow acceptors is much less clear. While there are reports of electronic Raman scattering, and calculations of the binding energy, of $1\Gamma_7^+$ for aluminum, gallium, and indium, the experimental results for these other acceptors are much less convincing [17]. Given the utility of

electronic Raman scattering for observing this state in boron-doped silicon, Raman scattering using below-gap excitation in suitable samples doped with these other acceptors would be highly desirable.

ACKNOWLEDGMENTS

This work was supported by the Natural Sciences and Engineering Research Council of Canada. We thank S. Pavlov for useful discussions.

[1] S. G. Pavlov, N. Dessmann, V. N. Shastin, R. K. Zhukavin, B. Redlich, A. F. G. van der Meer, M. Mittendorff, S. Winnerl, N. V. Abrosimov, H. Riemann, and H.-W. Hübers, Phys. Rev. X **4**, 021009 (2014).

[2] J. Salfi, J. A. Mol, D. Culcer, and S. Rogge, arXiv:1508.04259.

[3] E. Burstein, E. E. Bell, J. W. Davisson, and M. Lax, J. Phys. Chem. **57**, 849 (1953).

[4] B. Pajot, *Optical Absorption of Impurities and Defects in Semiconducting Crystals*, Springer Series in Solid-State Sciences, Vol. 158 (Springer, Berlin/Heidelberg, 2010).

[5] G. B. Wright and A. Mooradian, Phys. Rev. Lett. **18**, 608 (1967).

[6] G. B. Wright and A. Mooradian, in *Proceedings of the Ninth International Conference on the Physics of Semiconductors, Moscow, 1968* (Nauka, Leningrad, 1969), p. 1067.

[7] N. O. Lipari and A. Baldereschi, Solid State Commun. **25**, 665 (1978).

[8] R. Buczko and F. Bassani, Phys. Rev. B **45**, 5838 (1992).

[9] J. M. Cherlow, R. L. Aggarwal, and B. Lax, Phys. Rev. B **7**, 4547 (1973).

[10] T. N. Adam, R. T. Troeger, S. K. Ray, P.-C. Lv, and J. Kolodzey, Appl. Phys. Lett. **83**, 1713 (2003).

[11] N. O. Lipari, M. L. W. Thewalt, W. Andreoni, and A. Baldereschi, J. Phys. Soc. Jpn. **49** (Suppl. A), 165 (1980).

[12] N. O. Lipari, A. Baldereschi, and M. L. W. Thewalt, Solid State Commun. **33**, 277 (1980).

[13] M. L. W. Thewalt, Solid State Commun. **23**, 733 (1977).

[14] H. R. Chandrasekhar, A. K. Ramdas, and S. Rodriguez, Phys. Rev. B **12**, 5780 (1975).

[15] W. Scott and C. E. Jones, J. Appl. Phys. **50**, 7258 (1979).

[16] A. J. Mayur, M. D. Sciacca, A. K. Ramdas, and S. Rodriguez, Phys. Rev. B **48**, 10893 (1993).

[17] J. Serrano, A. Wysmolek, T. Ruf, and M. Cardona, Physica B (Amsterdam) **273–274**, 640 (1999).

[18] A. K. Ramdas and S. Rodriguez, Rep. Prog. Phys. **44**, 1297 (1981).

[19] M. Steger, A. Yang, D. Karaiskaj, M. L. W. Thewalt, E. E. Haller, J. W. Ager, M. Cardona, H. Riemann, N. V. Abrosimov, A. V. Gusev, A. D. Bulanov, A. K. Kaliteevskii, O. N. Godisov, P. Becker, and H.-J. Pohl, Phys. Rev. B **79**, 205210 (2009).

[20] C. E. Jones, D. Schafer, W. Scott, and R. J. Hager, J. Appl. Phys. **52**, 5148 (1981).

[21] J. J. Rome, W. C. Mitchel, G. J. Brown, D. W. Fischer, M. C. Ohmer, and T. L. Peterson, Appl. Phys. Lett. **41**, 254 (1982).

[22] P. A. Temple and C. E. Hathaway, Phys. Rev. B **7**, 3685 (1973).

[23] M. L. W. Thewalt, G. Kirczenow, R. R. Parsons, and R. Barrie, Can. J. Phys. **54**, 1728 (1976).

[24] V. A. Karasyuk, A. G. Steele, A. Mainwood, E. C. Lightowlers, G. Davies, D. M. Brake, and M. L. W. Thewalt, Phys. Rev. B **45**, 11736 (1992).

[25] K. Seeger, *Semiconductor Physics: An Introduction*, 4th ed., Springer Series in Solid-State Sciences No. 40 (Springer, Berlin/Heidelberg, 1989).

[26] B. Pajot, I. L. Beinikhes, S. M. Kogan, M. G. Novak, A. F. Polupanov, and C. Song, Semicond. Sci. Technol. **7**, 1162 (1992).